# Simultaneous prediction of velocity and angle-dependent reflectivity in time domain FWI

Ziguang Su, Daniel Trad, and Da Li


## ABSTRACT

Common-image gathers (CIGs) are essential for migration-based velocity analysis and amplitude-versus-angle (AVA) analysis, which could be utilized to predict lithology and fluid properties. Velocity is necessary for migration-based velocity analysis, and angle-dependent reflectivity is necessary for AVA analysis. To determine velocity and reflectivity for subsurface models, seismic inversion has been a conventional approach, followed by attribute calculation to aid interpretation. We present an iterative non-linear inversion method to simultaneously predict both velocity and amplitude-preserved angle-domain-common-image-gathers (ADCIGs). The key aspect of our technique is the extraction of angle information from the solution of a direction-vector-based wave equation in acoustic with density media. Because the extraction is solely dependent on the direction of wave propagation and is not dependent on acquisition coordinates, it can be applied to blended acquisition, which is another name for simultaneous seismic source acquisition. Our iterative inversion method is based on the time domain FWI using the nonlinear conjugate-gradient method. Throughout each iteration, the velocity model is sequentially updated at each reflection angle.


## INTRODUCTION

### Common image gather

A common image gather/CIG for a reflection point is a series of prestack migrated trace at the given image point (Jin et al., 2014), as shown in Figure 1.

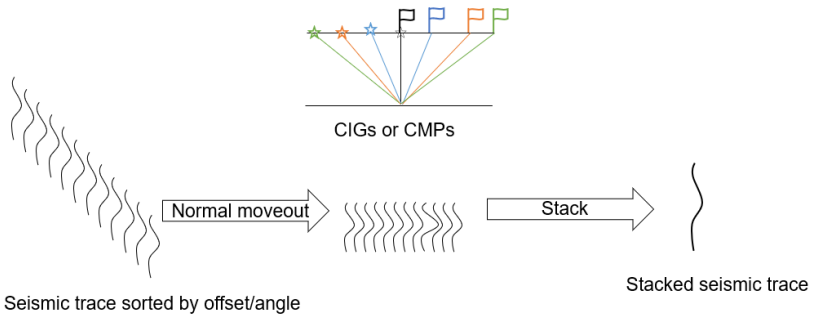


FIG. 1. common image gather

CIGs are the primary data for the techniques of amplitude variation with offset (AVO), or amplitude variation with incidence angle (AVA), which has been used to predict subsurface attribute interpretation for decades (Ostrander, 1984). CIGs can be extracted as a function of the subsurface attributes, such as subsurface offsets or reflection angles. CIGs taking offset are called offset-domain common-image gathers (ODCIGs).The offset in ODCIG normally refers to the distance between the shot and receiver on the surface. Later the

concept of offset was extended to the subsurface offset between the upgoing and downgoing wavefields (Rickett and Sava, 2002). Offset changes from a data-space parameter to a model-space parameter by migration. In a reflection raytrace, the subsurface offset is continuous as the depth increases.

The ODCIGs can be produced by either Kirchhoff migration or wavefield continuation migration (Sava and Fomel, 2003). However, ODCIGs fail to properly characterize commplex propagation path because of the ambiguity of reflector positions caused by multipathing(**?**).

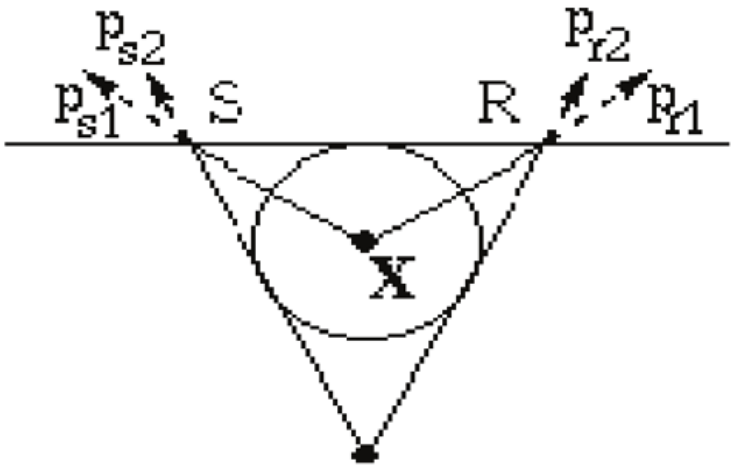


FIG. 2. In ODCIGs, two raypaths share the same source-receiver location and traveltime but different image point.

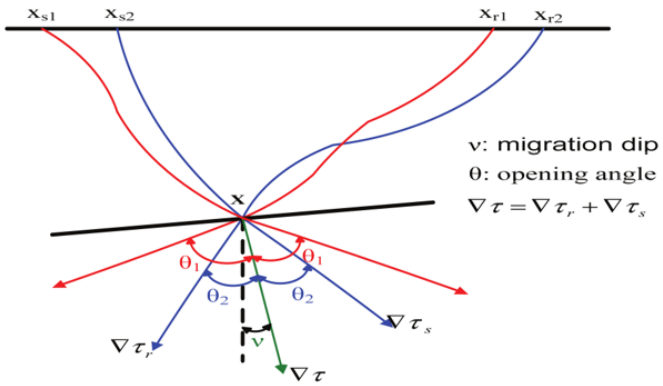


FIG. 3. In ODCIGs, two raypaths share the same subsurface offset and image point but different source-receiver locations. They have different raypath and reflection angles.

The problems in ODCIGs can be alleviated by ADCIGs. Similar to ODCIGs, the ADCIGs can also be produced by pre-imaging methods like Kirchhoff methods (Xu et al., 2001) or wave-equation methods (De Bruin et al., 1990). These two methods are based on the wave equation, so there's no sensitivity to the ray-traced angle. The ADCIGs can also be computed after-imaging (Biondi and Shan, 2002; Rickett and Sava, 2002) or transferred from ODCIG by Fourier Transform (Sava and Fomel, 2003).

## AVA response in elastic and acoustic media

The AVA response in elastic media can be described as Knott-Zoeppritz equations (Aki and Richards, 2002). The assumption of continuity of displacement and traction across an elastic boundary has led to four equations relating all relevant displacement amplitudes above and below the boundary. In our terminology (see Figure 4) these equations relate $P_I$, $S_I$, etc. as follows (Innanen, 2011):

$$\begin{cases} \sin\theta_0\left(P_{\mathrm{I}}+P_{\mathrm{R}}\right)+\cos\phi_0\left(S_{\mathrm{I}}+S_{\mathrm{R}}\right)=\sin\phi_1\left(P_{\mathrm{T}}+P'_{\mathrm{I}}\right)+\cos\phi_1\left(S_{\mathrm{T}}+S'_{\mathrm{I}}\right), \\ \cos\theta_0\left(P_{\mathrm{I}}-P_{\mathrm{R}}\right)-\sin\phi_0\left(S_{\mathrm{I}}-S_{\mathrm{R}}\right)=\cos\phi_1\left(P_{\mathrm{T}}-P'_{\mathrm{I}}\right)-\sin\phi_1\left(S_{\mathrm{T}}-S'_{\mathrm{I}}\right), \\ 2\rho_0\left(V_{S_0}^2/V_{P_0}\right)\sin\theta_0\cos\theta_0\left(P_{\mathrm{I}}-P_{\mathrm{R}}\right)-\rho_0 V_{S_0}\left[1-2\left(V_{S_0}^2/V_{P_0}^2\right)\sin^2\theta_0\right]\left(S_{\mathrm{I}}-S_{\mathrm{R}}\right) \\ =2\rho_1\left(V_{S_1}^2/V_{P_0}\right)\sin\theta_0\cos\theta_0\left(P_{\mathrm{T}}-P'_{\mathrm{I}}\right)+\rho_1 V_{S_1}\left[1-2\left(V_{S_1}^2/V_{P_0}^2\right)\sin^2\theta_0\right]\left(S_{\mathrm{T}}-S'_{\mathrm{I}}\right), \\ \rho_0 V_{P_0}\left[1-2\left(V_{S_0}^2/V_{P_0}^2\right)\sin^2\theta_0\right]\left(P_{\mathrm{I}}-P_{\mathrm{R}}\right)-2\rho_0\left(V_{S_0}^2/V_{P_0}\right)\sin\theta_0\cos\phi_0\left(S_{\mathrm{T}}+S'_{\mathrm{I}}\right) \\ =\rho_1 V_{P_1}\left[1-2\left(V_{S_1}^2/V_{P_0}^2\right)\sin^2\theta_0\right]\left(P_{\mathrm{T}}+P'_{\mathrm{I}}\right)-2\rho_1\left(V_{S_1}^2/V_{P_0}\right)\sin\theta_0\cos\phi_1\left(S_{\mathrm{T}}+S'_{\mathrm{I}}\right). \end{cases} \tag{1}$$

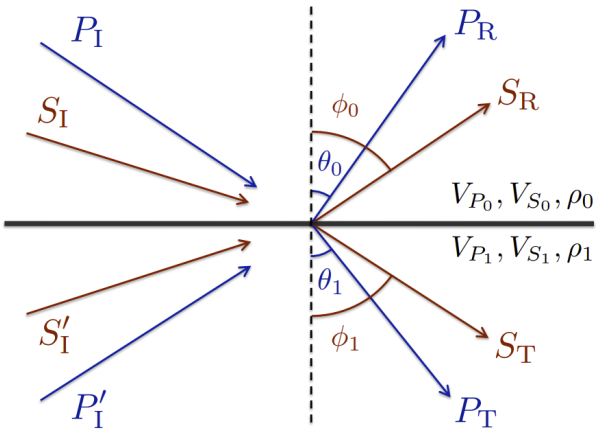


FIG. 4. Displacement amplitudes associated with the Knott-Zoeppritz equations.

The AVA response in acoustic media can be described as (Innanen, 2014):

$$R(\theta)=\frac{1-\Omega(\theta)}{1+\Omega(\theta)} \tag{2}$$

where

$$\Omega(\theta)=\left(\frac{\rho_0}{\rho_1}\right)\sqrt{\frac{\kappa_0}{\kappa_1}\frac{\rho_1}{\rho_0}}\left(\frac{1}{\cos\theta}\right)\sqrt{1-\frac{\kappa_1}{\kappa_0}\frac{\rho_0}{\rho_1}\sin^2\theta}. \tag{3}$$

$\rho$ is density and $\kappa$ is acoustic impedance, as shown in Figure 5.

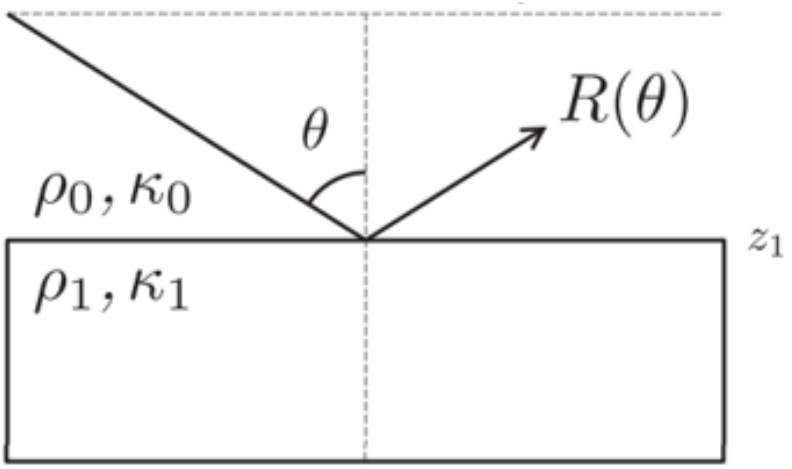


FIG. 5. Displacement amplitudes associated with tAVA response in acoustic media.

If a media only has a velocity as its physical property, it's called an acoustic medium and only has one wavefield $P$ in the wave propagation, as shown in equation:

$$\nabla^2 P - \frac{1}{c^2}\frac{\partial^2}{\partial t^2}P = 0 \tag{4}$$

where $P$ is the potential, and $c$ is the velocity.

If a medium has P wave velocity, S wave velocity and density as its physical properties, it can be considered an elastic medium. For 2D wave propagation, the elastic wave eqaution can be simulated using staggered grid Finite-difference method(Virieux, 1986a).

$$\begin{aligned}
\frac{\partial v_x}{\partial t} &= \frac{1}{\rho}(\frac{\partial \sigma_{xx}}{\partial x} + \frac{\partial \sigma_{xz}}{\partial z}),\\
\frac{\partial v_z}{\partial t} &= \frac{1}{\rho}(\frac{\partial \sigma_{zz}}{\partial z} + \frac{\partial \sigma_{xz}}{\partial x}),\\
\frac{\partial \sigma_{xx}}{\partial t} &= (\lambda + 2\mu)\frac{\partial v_x}{\partial x} + \lambda\frac{\partial v_z}{\partial z},\\
\frac{\partial \sigma_{zz}}{\partial t} &= (\lambda + 2\mu)\frac{\partial v_z}{\partial z} + \lambda\frac{\partial v_x}{\partial x},\\
\frac{\partial \sigma_{xz}}{\partial t} &= \mu(\frac{\partial v_z}{\partial x} + \frac{\partial v_x}{\partial z}),
\end{aligned} \tag{5}$$

where $\sigma_{xx}$and $\sigma_{zz}$ are the normal component of stress tensor, $\sigma_{xz}$ is the shear component, $\lambda$ is the $Lam\acute{e}$ parameter and $\mu$ is the rigidity. $\lambda$ and $\mu$ can be calculated through P wave velocity $v_p$, S wave velocity $v_s$ and density $\rho$.

If a medium has velocity and density as its physical properties, it can be considered an acoustic medium with density, or an elastic medium with only SH waves. The wave equation for this medium in 1D is:

$$\frac{\partial}{\partial x}(\frac{1}{\rho}\frac{\partial P}{\partial x}) - \frac{1}{\rho c^2}\frac{\partial^2}{\partial t^2}P = 0 \tag{6}$$

where $\rho$ is the density. If we replace $P$ with new variable,

$$\begin{cases} u = \frac{\partial P}{\partial t} \\ v = -\frac{1}{\rho}\frac{\partial P}{\partial x} \end{cases} \tag{7}$$

The equation 6 will become

$$\begin{cases} \frac{\partial u}{\partial t} = -\rho c^2 \frac{\partial v}{\partial x} \\ \frac{\partial v}{\partial t} = -\frac{1}{\rho}\frac{\partial P}{\partial x} \end{cases} \tag{8}$$

This form can be used in staggered grid Finite-difference method for wave propagation forward modeling. Extending the above equation in 3D, the wave equation 6 become

$$\frac{1}{\rho}\nabla^2 P^{'} - \frac{1}{c^2\rho}\frac{\partial^2 P^{'}}{\partial t^2} = 0 \tag{9}$$

it can be changed into

$$\nabla(\frac{1}{\rho}\nabla P^{'}) - \frac{1}{c^2\rho}\frac{\partial}{\partial t}\frac{\partial P^{'}}{\partial t} = 0 \tag{10}$$

If we replace $P^{'}$ with new variable

$$\begin{cases} P = \frac{\partial P^{'}}{\partial t} \\ \overrightarrow{v} = \frac{1}{\rho}\nabla P^{'} \end{cases} \tag{11}$$

The equation 10 will become

$$\begin{cases} \frac{\partial P}{\partial t} = -\rho c^2 \nabla \cdot \overrightarrow{v} \\ \frac{\partial \overrightarrow{v}}{\partial t} = -\frac{1}{\rho}\frac{\partial P}{\partial x} \end{cases} \tag{12}$$

This form can be used in staggered grid Finite-difference method for wave propagation forward modeling. If we take 2D , equation 12 will become

$$\begin{cases} \frac{\partial P}{\partial t} = -\rho c^2 (\frac{\partial v_x}{\partial x} + \frac{\partial v_z}{\partial z}) \\ \frac{\partial v_x}{\partial t} = -\frac{1}{\rho}\frac{\partial P}{\partial x} \\ \frac{\partial v_z}{\partial t} = -\frac{1}{\rho}\frac{\partial P}{\partial z} \end{cases} \tag{13}$$

**ADCIG extraction from RTM / two-way wave-equation migration**

There are many migration methods that can extract ADCIGs. Compared with the formulations of true amplitude Kirchhoff migration (Bleistein, 1987; Bleistein et al., 2001) and one-way wavefield migration (Zhang et al., 2005), true amplitude RTM is much simpler because the propagator itself naturally carries the correct propagation amplitude if the shot record is well approximated by solving the wave equation (Zhang and Sun, 2009). Because the RTM is based on the direct solutions of the wave equation, energy associated with multiple scatter events, steep drops and a broad range of wavenumbers will be preserved.

Methods for extracting angle-domain common-image gathers (ADCIGs) during 2D reverse-time migration fall into three main categories; direction-vector-based methods (DVB),

local-plane-wave decomposition methods (LPWD), and local-shift imaging condition methods (Jin et al., 2014).

The DVB method computes angles from defined vectors. The angle can either be the source and receiver wavefield propagation angle or the incident/reflection angle. There are many definitions for the vectors in the DVB method: the Poynting vector (Dickens and Winbow, 2011), polarization vector, instantaneous-wavenumber (Zhang and McMechan, 2011), energy norm (Rocha et al., 2016) etc. The DVB method is easy to compute and produces high angle resolution, but is not stable for complicated wavefields that contain overlapping events.

Let us take the Poynting vector in acoustic media as an example to show how the vectors are computed. The Poynting vector represents the directional energy flux of a wavefield (Stratton, 2007). The Poynting vector computation in acoustic wavefield is

$$\mathbf{S} = -\upsilon P = -\nabla P \frac{dP}{dt} P \tag{14}$$

where $\mathbf{S}$ is the Poynting vector, $-\upsilon$ is the velocity vector and $P$ is the stress wavefield (Cerveny, 2005). The $\mathbf{S}$ shares the same direction with the ray trace, so the angle between $\mathbf{S}_{source}$ and $\mathbf{S}_{receivers}$ is twice the value of reflection value.

$$cos2\theta = \frac{\mathbf{S}_{source}\mathbf{S}_{receivers}}{|\mathbf{S}_{source}||\mathbf{S}_{receivers}|} \tag{15}$$

where $\theta$ is the reflection angle. so the $\theta$ is

$$\theta = \frac{1}{2} arccos \frac{\mathbf{S}_{source}\mathbf{S}_{receivers}}{|\mathbf{S}_{source}||\mathbf{S}_{receivers}|} \tag{16}$$

In 2D, if we set the source stress wavefield as $P_s$ and receiver stress wavefield as $P_r$, the reflection angle $\theta$ turns into

$$\theta = \frac{1}{2} arccos \frac{\frac{\partial P_s}{\partial x}\frac{\partial P_r}{\partial x} + \frac{\partial P_s}{\partial z}\frac{\partial P_r}{\partial z}}{\sqrt{(\frac{\partial P_s}{\partial x})^2 + (\frac{\partial P_s}{\partial z})^2} + \sqrt{(\frac{\partial P_r}{\partial x})^2 + (\frac{\partial P_r}{\partial z})^2}} \tag{17}$$

and vector perpendicular to the reflection plane is

$$\mathbf{S} = (\mathbf{S}_{source} + \mathbf{S}_{receivers})/|cos2\theta| \tag{18}$$

The azimuth can also be computed, and in the 2D case, it is either $0^\circ$ or $180^\circ$. With the angle information, the common angle gather can be obtained after RTM without external computation. To get the ADCIG, the reflection angle $\theta$ is introduced in RTM's image condition from equation 5:

$$R(\overrightarrow{x}, \theta) = \int p_B(\overrightarrow{x}, \theta; t) p_F^{-1}(\overrightarrow{x}, \theta; t) dt \tag{19}$$

**Review of full waveform inversion in time domain**

In a standard FWI problem, we minimize a misfit function

$$\mathbf{E}(\mathbf{m}), \tag{20}$$

subject to

$$\mathbf{F}(\mathbf{m})\mathbf{u}(\mathbf{x},t) = \mathbf{s}(\mathbf{x},t), \tag{21}$$

where $\mathbf{E}$ is a function with respect of model parameters $\mathbf{m}$, $\mathbf{F}(\mathbf{m})$ characterizes the seismic wave equation, $\mathbf{u}(\mathbf{x},t)$ denotes the particle displacement at time $t \in [0,T]$ excited by an external source $\mathbf{s}(\mathbf{x},t)$ and $\mathbf{x}$ denotes spatial coordinates .

The wave equation $\mathbf{F}(\mathbf{m})$ in elastic media can be expressed as (Aki and Richards, 1980)

$$\mathbf{F}(\rho,\lambda,\mu) = \rho(\mathbf{x})\frac{\partial^2}{\partial t^2}[\cdot] - \nabla\cdot\left[\lambda(\nabla\cdot[\cdot])\mathbf{I} + \mu\left(\nabla[\cdot] + \nabla[\cdot]^T\right)\right],$$

where $[\,\cdot\,]$ is a place-holder for the variable acted upon by $\mathbf{F}(\mathbf{m})$ and $\mathbf{I}$ is the identity operator. $\rho$, $\lambda$ and $\mu$ denote density and the Lamé parameters. This elastic wave equation can be solved by the stagger-grid finite-difference scheme (Virieux, 1986b; Levander, 1988). The objective function taking the least-squares norm of the misfit vector $\Delta\mathbf{u}$ is given by

$$\begin{aligned}\mathbf{E}(\mathbf{m}) &= \frac{1}{2}\Delta\mathbf{u}^\dagger\Delta\mathbf{u} = \frac{1}{2}\left\|\mathbf{u}_{\text{obs}} - \mathbf{u}_{\text{syn}}\right\|^2 \\ &= \frac{1}{2}\left(\mathbf{u}_{\text{obs}} - \mathbf{u}_{\text{syn}}\right)^{\text{T}}\left(\mathbf{u}_{\text{obs}} - \mathbf{u}_{\text{cal}}\right) \\ &= \frac{1}{2}\sum_{s=1}^{N_s}\sum_{r=1}^{N_r}\int_T \left|u_{\text{obs}}\left(\mathbf{x}_r,t\right) - u_{\text{syn}}\left(\mathbf{x}_r,t;\mathbf{m}\right)\right|^2 \,\mathrm{d}t,\end{aligned} \tag{22}$$

where $\dagger$ denotes the adjoint operator (conjugate transpose), the data misfit $\Delta\mathbf{u}$ is defined by the differences between the observed seismic data $\mathbf{u}_{\text{obs}}$ and the synthetic seismic data $\mathbf{u}_{\text{syn}}$ recorded at the $r$-th receiver and generated by the $s$-th source $\mathbf{s}_s$ for model $\mathbf{m}$. $N_s$ and $N_r$ denote she number of sources and receivers.

Via the conjugate gradient method, the model is updated iteratively according to

$$\mathbf{m}_{k+1} = \mathbf{m}_k + \alpha_k\delta\mathbf{m}_k, \tag{23}$$

where $k$ is the iteration number, $\alpha$ the step length, and $\delta\mathbf{m}_k$ is a search direction or descent direction and can be derived from the gradient of the misfit function. The gradient of $\mathbf{E}(\mathbf{m})$ with respect to $\mathbf{m}$, $\nabla_m\mathbf{E}$, can be calculated efficiently using the adjoint-state method (Plessix, 2006):

$$\nabla_m\mathbf{E}(\mathbf{x}) = -\sum_{s=1}^{N_s}\int_T u^\dagger_{\text{obs}}\left(\mathbf{x},t\right)\cdot\frac{\partial\mathbf{F}}{\partial\mathbf{m}}u_{\text{obs}}\left(\mathbf{x},t\right)\mathrm{d}t. \tag{24}$$

where $u^\dagger_{\text{obs}}$ is the adjoint wavefield.

### True amplitude RTM

RTM is a migration method that is based on the two-way wave equation. Compared with migration methods based on the one-way wave equation, RTM has better results for complex structures like salt structures. RTM is initially introduced by many authors (Baysal et al., 1983; Whitmore, 2005; McMECHAN, 1983).

To migrate a shot gather $Q(x, y; x_s, y_x; t)$ using conventional RTM, we need to compute wavefields shot at the source location and seismic traces recorded at the receiver location, with a source at $(x_s, y_s, z_s = 0)$ and receivers at $(x, y, z = 0)$. The two-way acoustic wave equation goes:

$$(\frac{1}{c^2}\frac{\partial^2}{\partial t^2}p_F(\overrightarrow{x};t) = \delta(\overrightarrow{x} - \overrightarrow{x_s})f(t) \tag{25}$$

and

$$\begin{cases}(\frac{1}{c^2}\frac{\partial^2}{\partial t^2} - \nabla^2)p_B(\overrightarrow{x};t) = 0\\ p_B(x, y.z = 0; t) = Q(x, y; x_s, y_x; t)\end{cases} \tag{26}$$

where $p_F$ and $p_B$ are forward wavefield and backward wavefield respectively, $c = c(x, y, z)$ is the velocity, $f(t)$ is the wavelet function, and $\nabla^2$ is the Laplacian operator.

To get a common shot image with correct migration amplitude, we need to apply "deconvolution" image conditions(ICs)(Zhang et al., 2005):

$$R(\overrightarrow{x}) = \int p_B(\overrightarrow{x};t)p_F^{-1}(\overrightarrow{x};t)dt \tag{27}$$

This IC is simple to apply in frequency domain for one-way wave equation migration. However, it's difficult to apply in time domain RTM. In practice, the "cross-correlation" is often preferable for the reason of stability.

$$R(\overrightarrow{x}) = \int p_B(\overrightarrow{x};t)p_F^(\overrightarrow{x};t)dt \tag{28}$$

Although this IC doesn't appear to be consitent with the true-amplitude migration, a modified IC from equation 25 can be used to obtain true-amplitude angle gathers (Zhang et al., 2007).

$$\begin{cases}(\frac{1}{c^2}\frac{\partial^2}{\partial t^2} - \nabla^2)p_F(\overrightarrow{x};t) = 0\\ p_B(x, y.z = 0; t) = \delta(\overrightarrow{x} - \overrightarrow{x_s})\int_0^t f(t')dt'\end{cases} \tag{29}$$

If we set Ricker wavelet as the source wavelet.

$$f(t) = [1 - 2\pi^2 f^2(t - \frac{1}{f})^2]e^{-\pi^2 f^2(t-\frac{1}{f})^2} \tag{30}$$

The Ricker wavelet is a normalized second derivitive of the Gaussian distribution, so the source function in equation 29 will be

$$\int_0^t f(t')dt' = (t - \frac{1}{f})e^{-\pi^2 f^2(t-\frac{1}{f})^2} \tag{31}$$

### Blended acquisiton

The blended acquisition technique targets at removing the limitation of no interference between adjacent shots by allowing sources to be shot simultaneously (Berkhout et al., 2009). While conventional acquisitions record energy coming from only one source at a time, blended acquisitions record energy coming from multiple sources simultaneously (Garottu, 1983; Beasley et al., 1998; Berkhout, 2008), as shown in Figure 6.

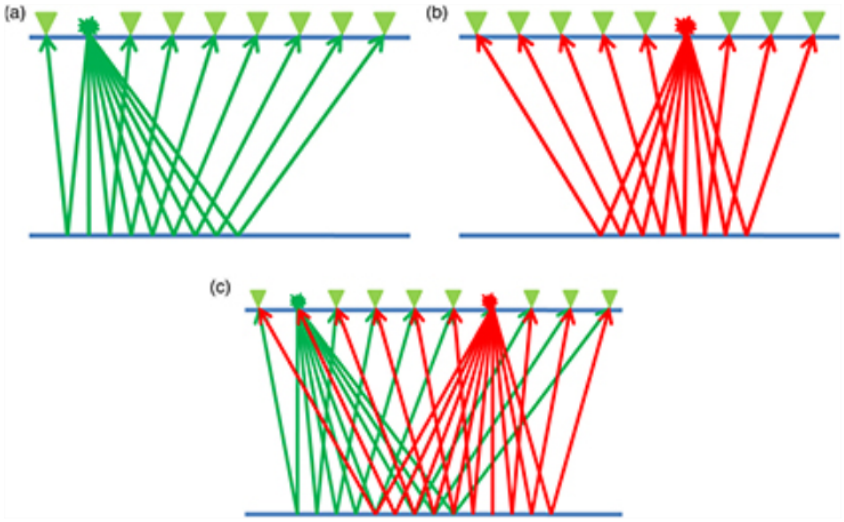


FIG. 6. (a) and (b) are illustrations of conventional single shot acquisition and (c) is blended shot acquisition.

When seismic sources are acquired simultaneously, data quality is improved (e.g., through denser shooting) and acquisition costs are reduced. This is possible because simultaneous seismic source acquisition permits temporal overlap between shot recordings (e.g., efficient wide-azimuth shooting).

## METHOD

### Hypotheses

1. The earth's response can generally be approximated as linear and any response to any complex force can be calculated as a sum of the displacement of constituent body forces. Similarly, the response to multiple seismic sources can be considered a sum of responses to each independent source.
2. There is only one wave direction per image point per image time. (Vyas et al., 2011)
3. The AVA response curve is continuous when the angle interval is relatively small.

### Wave propagation direction for ADCIGs

In acoutic media, the model property is $Vp$, P wave velocity, and there's only one scalar wavefield $P$. The spatial gradient of the wavefield $P$, which includes the Poynting vector

and the polarization direction $\Delta P$, is used to determine the direction of wave propagation.

The model properties in acoustic with density media are $Vp$ and $density$. Scalar wavefield $P$ and vector wavefield $\overrightarrow{v}$ are the wavefields. The wave propagates directly in the direction $\overrightarrow{v}$, with an amplitude of $P$. Reflectivity is obtained from impedance, which can be generated by the model properties $Vp$ and $density$.

There are also other modified wave equations to get reflectivity, like (Whitmore et al., 2020)

$$\frac{\partial^2 P}{\partial t^2} - [V^2 \nabla^2 P + V \nabla V \cdot \nabla P - 2V^2 (R \cdot \nabla P)] = S \tag{32}$$

where $R$ is reflectivity, $\nabla V$ is spatial derivitive of velocity model.

But unlike equation 13 which naturally has vector wavefield, these kind of method still rely on spatial gradient of scalar wavefield to derive propagation direction.

The ADCIGs extraction method is based on direction vector of the image point and irrelevant of the acquisition coordinates. So the ADCIGs method can be applied to blended data as well. For unblended data, the signal in source and receiver wavefield corespond to each other, as shown in Figure 7. Regarding the blended data, as Figure 8 illustrates, crosstalk between the incorrect pair of source and receivers will result from the cross-correlation of RTM image condition if energy from different sources arrives at different times. Noise will be increased by other sources' crosstalk. We will take into consideration at each reflection angle in ADCIGs to reduce the crosstalk. The reflection amplitude at an image point is proportional to the incident amplitude for a given reflection angle. The ratio remains constant regardless of the acquisition coordinates. Nonetheless, the optimal source and receiver signal pair is always indicated by the cross-correlation's maximum value.

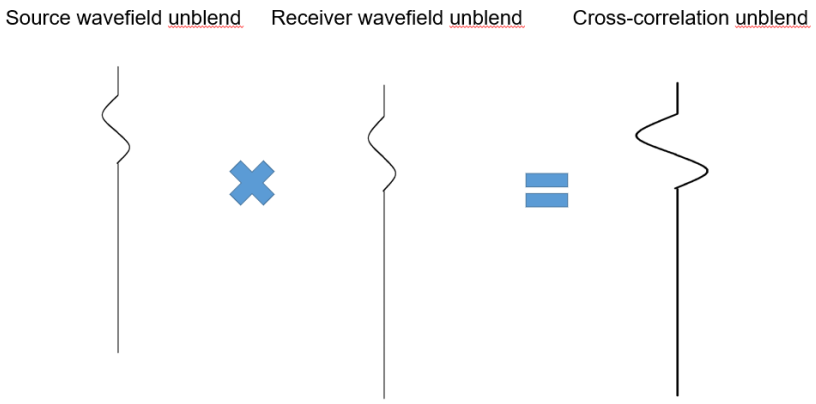


FIG. 7. Cross-correlation of source and receiver wavefield for unblended data

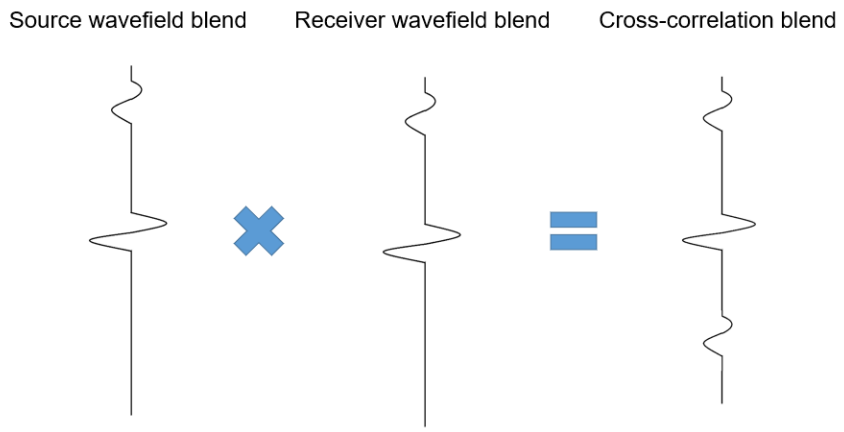


FIG. 8. Cross-correlation of source and receiver wavefield for blended data

## Time domain FWI and angle gathers

A conventional time domain FWI can be expressed (Yang et al., 2015)

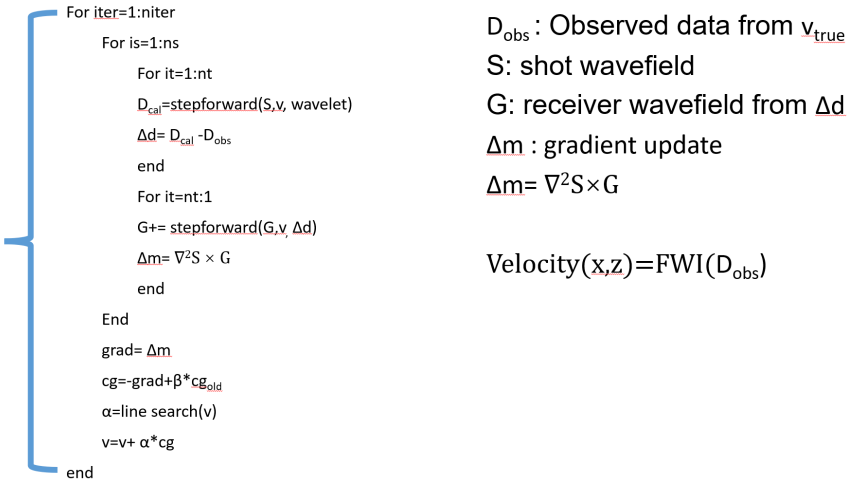


FIG. 9. Pseudo code of time domain FWI

The iterative optimization is nonlinear conjugate gradient method, and the step-size is determined by a line search algorithm.

We add ADCIGs into the time domain FWI. It can be seen that inside each iteration that the velocity model is update at each reflection angle. The model is updated in small reflenction angle first, then the updated model from small reflection angle is used for large angle. There are different stepsize for each angle at every iteration.

```
For iter=1:niter
    For is=1:ns
        For it=1:nt
            D_cal=stepforward(S,v,
            wavelet)
            Δd= D_cal -D_obs
        end
        For it=nt:1
            G+= stepforward(G,v, Δd)
            Δm (x,z,Θ) = ADCIG(∇²S,G)
        end
    End

    For i Θ =1:n Θ
        grad= Δm(i Θ) % read from Δm
        cg(i Θ)=-grad+β × cg_old(i Θ)
        α=line search(v)
        v=v+ α × cg
    end
end
```

FIG. 10. Pseudo code of anlge domain FWI

## RESULTS AND DISCUSSION

We are using a cutted marmousi model as our true velocity model. The model is 130 times 350 points and bin interval is 5 meters. The density model is homogenous contant model with the same size.

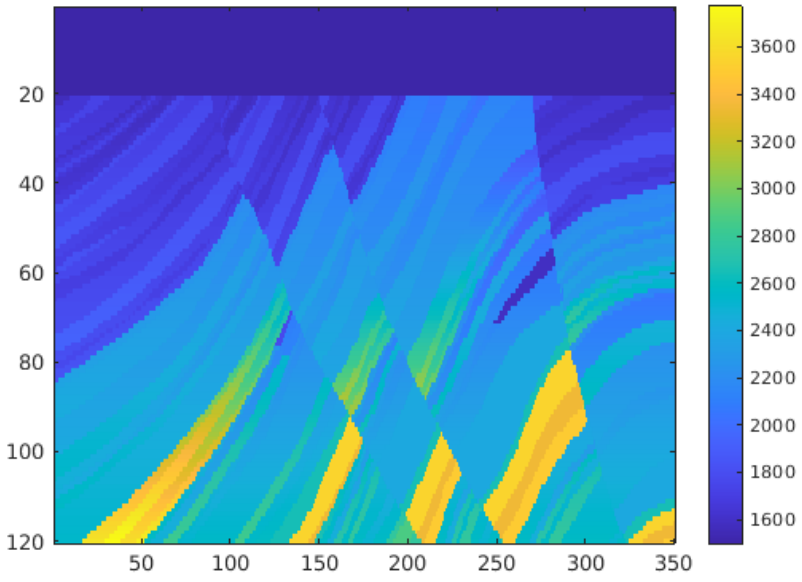


FIG. 11. True velocity model

The smoothed velocity model is taken as initial model.

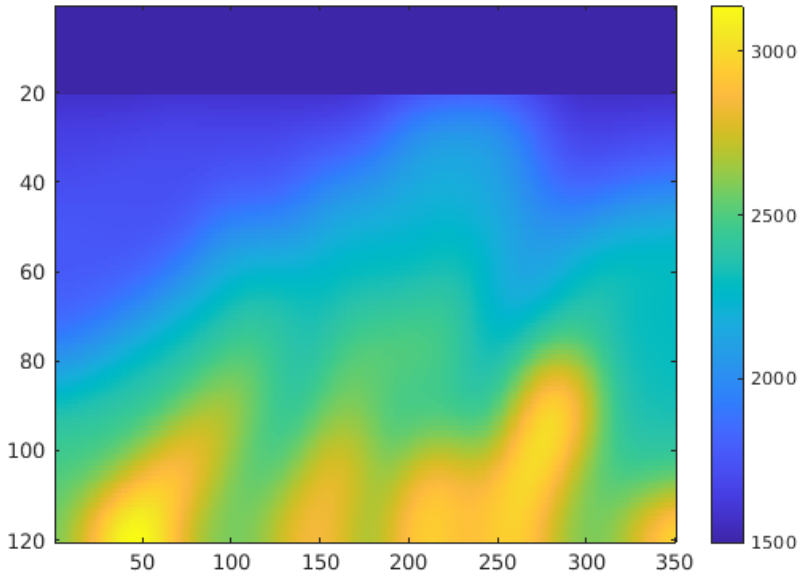


FIG. 12. Initial velocity model

Using conventional time domain FWI, the velocity model after 10 iteration is

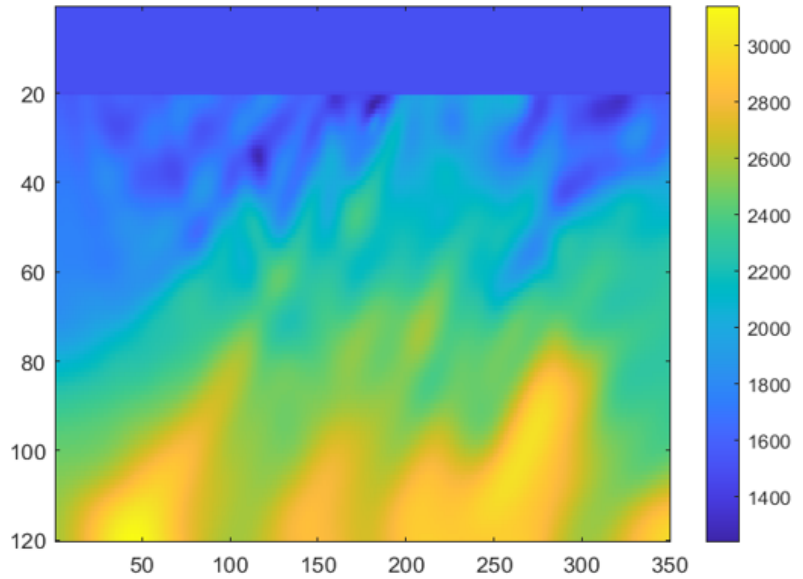


FIG. 13. The velocity model after 10 iteration

It can be seen that shallow subsurface structure has been updated.

For the angle domain FWI, in the first iteration, the 0-30, 36-60, 60-90 degree reflection angle velocity models are:

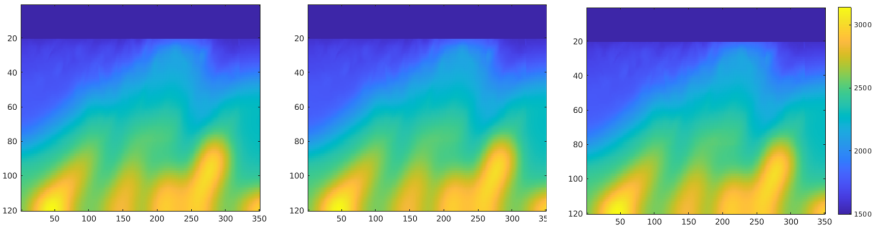

FIG. 14. The velocity model with the 0-30, 36-60, 60-90 degree reflection angle at 1 iteration

In the 9th iteration:

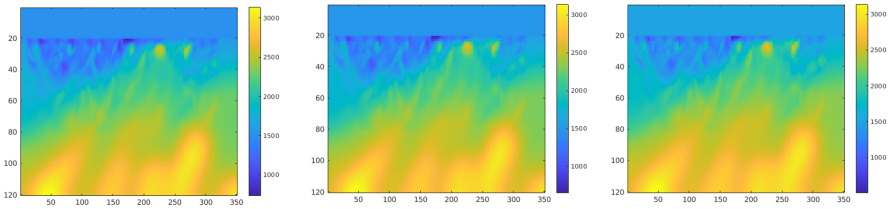

FIG. 15. The velocity model with the 0-30, 36-60, 60-90 degree reflection angle at 9 iteration

The small reflection angle velocity model has higher amplitude.

The unblended and blended velocity model from angle domain FWI in the 20th iteration is

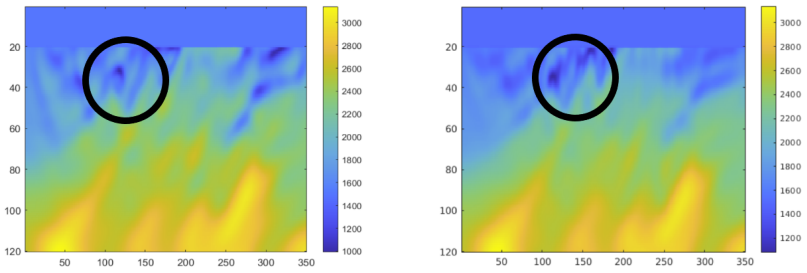

FIG. 16. The left is unblended velocity and on the right is blended velocity

It can be seen that the general trend of unblended and blended velocity looks alike, but the blended one is worse in the sharp contrast part in the black circle.

In order to compare the AVA information from angle domain FWI, we pick a point at the velocity model:

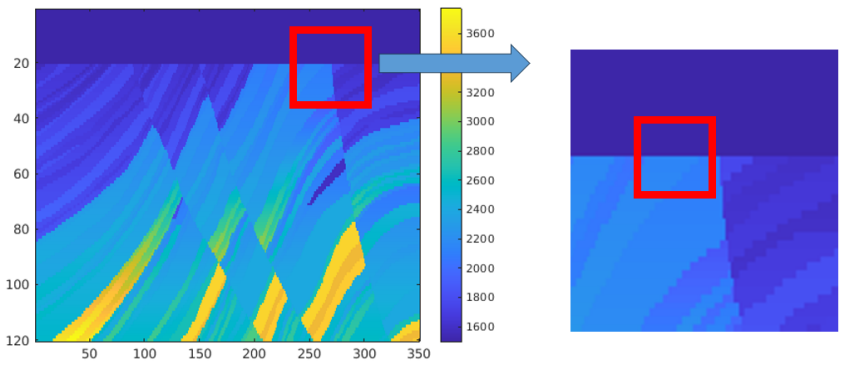


FIG. 17. The location of AVA information in velocity model

The result of the AVA response is

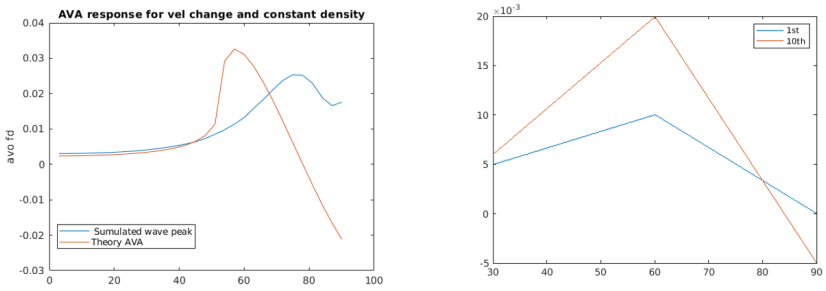


FIG. 18. On the left is the contrast of the theory and simulated AVA response at the image point, on the right is the AVA information from the angle domain FWI in 1st and 10th iteration

In the left of the Figure 18, we plotted the the theory and simulated AVA response at the image point, the peak of the reflection angle is different. One possible reason is that theory AVA is for plane wave source, not spherical wave. The AVA response from angle domain FWI fits the trend of the theory AVA response.

## CONCLUSIONS

Aamplitude variation with angle /AVA information can be extracted from ADCIGs . RTM / two-way wave-equation migration is used for ADCIGs extraction. Wave-equation migration with velocity and reflectivity are updated simultaneously in acoustic media with density. The simultaneous prediction of velocity and angle-dependent reflectivity in time domain FWI could be used in blended data.

The ADCIGs have been demonstrated to be amplitude-preserved and hence suited for more complicated models after comparing the AVA response with the Zoeppritz equations and simulating forward modelling in a layered model. We can also use our ADCIGs to retrieve data from blended acquisition. The AVA response from blended data processed using the direct migration approach displays attributes similar to those of unblended data, proving that our ADCIG extraction method is fairly effective for blended acquisition.

## FUTURE WORK

### 3D applications

Despite the high cost, 3D seismic surveys have many advantages compared with 2D surveys. 3D seismic acquisitions provide a volume of closely spaced seismic data in three dimensions. In contrast, the 2D seismic survey provides a slice of data in two dimensions. Therefore, 3D has a wider field coverage than 2D. Moreover, 3D seismic surveys enhance the signal-to-noise ratio (S/N) significantly (Gaarenstroom, 1984).

In the 2D seismic acquisition, the data is 3D: time, receiver coordinates, and shots coordinates. We could deblend blended shots by transferring data from the shots domain to other domains like the receiver domain, offset domain, and angle domain. The target shot will be coherent, while other shots will be incoherent. However, in a 3D seismic survey, there are five dimensions to represent data in minimum space: inline, crossline, offset, azimuth, and time (other parameterizations are also possible). Deblending through multiple domain transform is difficult because different domains are connected through complex physics. Nevertheless, I believe changing domains will make shots other than shots incoherent since only the target shot has the correct header and time shift.

## ACKNOWLEDGMENTS

The sponsors of CREWES are gratefully thanked for continued support. This work was funded by CREWES industrial sponsors, NSERC (Natural Science and Engineering Research Council of Canada) through the grant CRDPJ 543578-19.

## REFERENCES

Aki, K., and Richards, P., 2002, Quantitative seismology, 2nd ed[]: University Science Books.

Aki, K., and Richards, P. G., 1980, Quantitative seismology: W.H. Freeman & Co.

Baysal, E., Kosloff, D. D., and Sherwood, J. W. C., 1983, Reverse time migration: GEOPHYSICS, **48**, No. 11, 1514–1524.

Beasley, C. J., Chambers, R. E., and Jiang, Z., 1998, A new look at simultaneous sources, *in* SEG Technical Program Expanded Abstracts 1998, Society of Exploration Geophysicists, 133–135.

Berkhout, A., 2008, Changing the mindset in seismic data acquisition: The Leading Edge, **27**, No. 7, 924–938.

Berkhout, A., Verschuur, D., and Blacquière, G., 2009, Seismic imaging with incoherent wavefields, *in* 2009 SEG Annual Meeting, OnePetro.

Biondi, B., and Shan, G., 2002, Prestack imaging of overturned reflections by reverse time migration, Society of Exploration Geophysicists: SEG Technical Program Expanded Abstracts 2002, 1284–1287.

Bleistein, N., 1987, On the imaging of reflectors in the earth: Geophysics, **52**, No. 7, 931–942.

Bleistein, N., Cohen, J. K., Stockwell Jr, J. W., and Berryman, J., 2001, Mathematics of multidimensional seismic imaging, migration, and inversion. interdisciplinary applied mathematics, vol 13: Appl. Mech. Rev., **54**, No. 5, B94–B96.

Cerveny, V., 2005, Seismic ray theory: Cambridge university press.

De Bruin, C., Wapenaar, C., and Berkhout, A., 1990, Angle-dependent reflectivity by means of prestack migration: Geophysics, **55**, No. 9, 1223–1234.

Dickens, T. A., and Winbow, G. A., 2011, Rtm angle gathers using poynting vectors, *in* SEG Technical Program Expanded Abstracts 2011, Society of Exploration Geophysicists, 3109–3113.

Gaarenstroom, L., 1984, The value of 3d seismic in field development: SPE Annual Technical Conference and Exhibition.

Garottu, R., 1983, Simultaneous recording of several vibroseis® seismic lines, Society of Exploration Geophysicists: SEG Technical Program Expanded Abstracts 1983, 308–310.

Innanen, K., 2011, Matrix forms for the knott-zoeppritz equations.

Innanen, K. A., 2014, Seismic avo and the inverse hessian in precritical reflection full waveform inversion: Geophysical Journal International, **199**, No. 2, 717–734.

Jin, H., McMechan, G. A., and Guan, H., 2014, Comparison of methods for extracting adcigs from rtm: Geophysics, **79**, No. 3, S89–S103.

Levander, A. R., 1988, Fourth-order finite-difference p-sv seismograms: Geophysics, **53**, No. 11, 1425–1436.

McMECHAN, G. A., 1983, Migration by extrapolation of time-dependent boundary values*: Geophysical Prospecting, **31**, No. 3, 413–420.

Ostrander, W., 1984, Plane-wave reflection coefficients for gas sands at nonnormal angles of incidence: Geophysics, **49**, No. 10, 1637–1648.

Plessix, R.-E., 2006, A review of the adjoint-state method for computing the gradient of a functional with geophysical applications: Geophysical Journal International, **167**, No. 2, 495–503.

Rickett, J. E., and Sava, P. C., 2002, Offset and angle-domain common image-point gathers for shot-profile migration: Geophysics, **67**, No. 3, 883–889.

Rocha, D., Tanushev, N., and Sava, P., 2016, Isotropic elastic wavefield imaging using the energy norm: Geophysics, **81**, S207–S219, `http://dx.doi.org/10.1190/geo2015-0487.1`.
URL `http://dx.doi.org/10.1190/geo2015-0487.1`

Sava, P. C., and Fomel, S., 2003, Angle-domain common-image gathers by wavefield continuation methods: Geophysics, **68**, No. 3, 1065–1074.

Stratton, J. A., 2007, Electromagnetic theory, vol. 33: John Wiley & Sons.

Virieux, J., 1986a, P-SV wave propagation in heterogeneous media: velocity-stress finite-difference method: Geophysics, **51**, 889–901.

Virieux, J., 1986b, P-sv wave propagation in heterogeneous media: Velocity-stress finite-difference method: Geophysics, **51**, No. 4, 889–901.

Vyas, M., Nichols, D., and Mobley, E., 2011, Efficient rtm angle gathers using source directions, *in* 2011 SEG Annual Meeting, OnePetro.

Whitmore, N., Ramos-Martinez, J., Yang, Y., and Valenciano, A., 2020, Full wavefield modeling with vector reflectivity, *in* EAGE 2020 Annual Conference & Exhibition Online, vol. 2020, European Association of Geoscientists & Engineers, 1–5.

Whitmore, N. D., 2005, Iterative depth migration by backward time propagation: SEG Technical Program Expanded Abstracts 1983, 382–385, `https://library.seg.org/doi/pdf/10.1190/1.1893867`.
URL `https://library.seg.org/doi/abs/10.1190/1.1893867`

Xu, S., Chauris, H., Lambaré, G., and Noble, M., 2001, Common-angle migration: A strategy for imaging complex media: Geophysics, **66**, No. 6, 1877–1894.

Yang, P., Gao, J., and Wang, B., 2015, A graphics processing unit implementation of time-domain full-waveform inversion: Geophysics, **80**, No. 3, F31–F39.

Zhang, Q., and McMechan, G. A., 2011, Common-image gathers in the incident phase-angle domain from reverse time migration in 2d elastic vti media: Geophysics, **76**, No. 6, S197–S206.

Zhang, Y., and Sun, J., 2009, Practical issues in reverse time migration: True amplitude gathers, noise removal and harmonic source encoding: First break, **27**, No. 1.

Zhang, Y., Xu, S., Bleistein, N., and Zhang, G., 2007, True-amplitude, angle-domain, common-image gathers from one-way wave-equation migrations: Geophysics, **72**, No. 1, S49–S58.

Zhang, Y., Zhang, G., and Bleistein, N., 2005, Theory of true-amplitude one-way wave equations and true-amplitude common-shot migration: Geophysics, **70**, No. 4, E1–E10.